**RESEARCH ARTICLE**

ADVANCED ENERGY MATERIALS
www.advenergymat.de

# Correlating the Hybridization of Local-Exciton and Charge-Transfer States with Charge Generation in Organic Solar Cells

*Deping Qian,* Saied Md Pratik, Qi Liu, Yifan Dong, Rui Zhang, Jianwei Yu, Nicola Gasparini, Jiaying Wu, Tiankai Zhang, Veaceslav Coropceanu, Xia Guo, Maojie Zhang,* Jean-Luc Bredas, Feng Gao, and James R. Durrant**

**In organic solar cells with very small energetic-offset ($\Delta E_{LE-CT}$), the charge-transfer (CT) and local-exciton (LE) states strongly interact via electronic hybridization and thermal population effects, suppressing the non-radiative recombination. Here, we investigated the impact of these effects on charge generation and recombination. In the blends of PTO2:C8IC and PTO2:Y6 with very small, ultra-fast CT state formation was observed, and assigned to direct photoexcitation resulting from strong hybridization of the LE and CT states (i.e., LE-CT intermixed states). These states in turn accelerate the recombination of both CT and charge separated (CS) states. Moreover, they can be significantly weakened by an external-electric field, which enhanced the yield of CT and CS states but attenuated the emission of the device. This study highlights that excessive LE-CT hybridization due to very low , whilst enabling direct and ultrafast charge transfer and increasing the proportion of radiative versus non-radiative recombination rates, comes at the expense of accelerating recombination losses competing with exciton-to-charge conversion process, resulting in a loss of photocurrent generation.**

## 1. Introduction

The power conversion efficiencies (PCE) of single-junction organic solar cells (OSCs) have currently been pushed to 19%.[1–5] One of the breakthroughs accounting for this striking progress in the PCEs of OSCs has been decreasing the energetic offset ($\Delta E_{LE-CT}$) values between charge-transfer (CT) and local-exciton (LE) states at the donor-acceptor (D-A) interface.[6,7] This design strategy has not only successfully minimized the energy loss associated with photoinduced charge transfer, but also induced new photophysical concepts that differ from those describing the conventional polymer:fullerene materials.[6,8,9] To date, intensive research has been devoted to studying the correlations between device optoelectronic properties and those newly observed photophysics.[9–11]

---

D. Qian
Straits Institute of Flexible Electronics (SIFE, Future Technologies)
Fujian Normal University
Fuzhou, Fujian 350117, China
E-mail: ifedpqian@fjnu.edu.cn

D. Qian
Straits Laboratory of Flexible Electronics (SLoFE)
Fuzhou, Fujian 350117, China

D. Qian, Y. Dong, N. Gasparini, J. Wu, J. R. Durrant
Department of Chemistry and Centre for Processable Electronics
Imperial College London
London W12 0BZ, UK
E-mail: j.durrant@imperial.ac.uk

The ORCID identification number(s) for the author(s) of this article can be found under https://doi.org/10.1002/aenm.202301026

**DOI: 10.1002/aenm.202301026**

S. M. Pratik, V. Coropceanu, J.-L. Bredas
Department of Chemistry and Biochemistry
The University of Arizona
Tucson, AZ 85721-0088, USA

Q. Liu, X. Guo, M. Zhang
National Engineering Research Center for Colloidal Materials, School of Chemistry & Chemical Engineering
Shandong University
Jinan, Shandong 250100, China
E-mail: mjzhang@sdu.edu.cn

R. Zhang, J. Yu, T. Zhang, F. Gao
Department of Physics, Chemistry and Biology (IFM)
Linköping University
Linköping 58183, Sweden

J. R. Durrant
Department of Materials Science and Engineering
Swansea University
Swansea SA1 8EN, UK

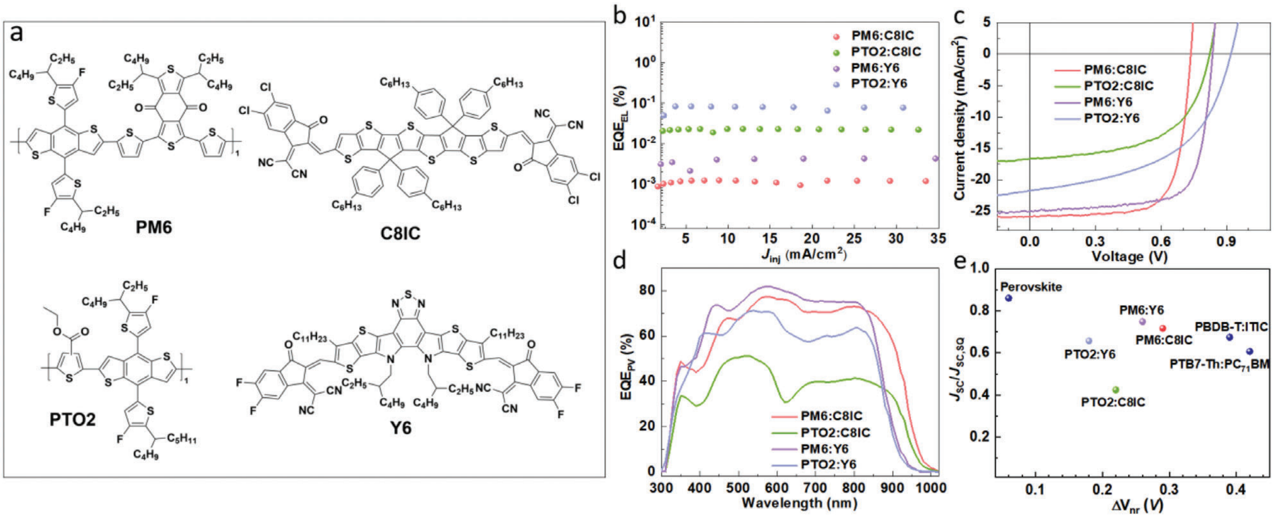

**Figure 1.** a) Chemical structures of the electron donors (PM6 and PTO2) and electron acceptors (C8IC and Y6) studied in this work. b) $EQE_{EL}$ as a function of injected current density, c) current-voltage ($J$–$V$) characteristics, and d) $EQE_{PV}$ spectra of the devices based on PM6:C8IC, PTO2:C8IC, PM6:Y6, and PTO2:Y6. The $EQE_{EL}$ values of the devices are extracted from (b), where the injected current densities ($J_{inj}$) are comparable to the short-circuit current densities of the devices. e) Charge generation efficiency ($J_{SC}/J_{SC,SQ}$) versus $\Delta V_{nr}$.

When the CT state energy is substantially lower than that of the LE states of the D or A molecules, a two-state model including the CT state coupled with the ground state ($S_0$) has been widely utilized for the description of the optical transitions and non-radiative recombination processes following exciton dissociation (we note that, here, the term "CT state" generally refers to charge pairs generated by charge transfer at the donor/acceptor interface, rather than to states localized (bound) at the interface by their Coulomb attraction).[12,13] Ultra-fast charge transfer and separation processes take place via these CT states.[14] However, when the CT and LE states are close in energy, the role of the highly emissive and localized exciton state must be considered in the competing charge recombination pathways, as the CT state can interact with the LE state through electronic hybridization and/or thermal population.[6,12] Thus, instead of only the CT states, such intermixed LE-CT states can govern the photoelectric conversion properties of D-A blend films with a small $\Delta E_{LE-CT}$.[15]

Since the charge-to-photon conversion ability of a device correlates with its voltage loss, it is striking that recent advances in materials and device design with low $\Delta E_{LE-CT}$ have led to OSCs where the non-radiative voltage loss ($\Delta V_{nr}$) was reduced to as little as 0.13 V.[16] At the same time, it has been reported that exciton dissociation in those small $\Delta E_{LE-CT}$ cases occurred at a much slower rate than in larger $\Delta E_{LE-CT}$ systems.[6] For extreme cases with $\Delta E_{LE-CT}$ being close to 0 eV, it was found that the quantum yield of free-carrier generation ($EQE_{PV}$) in an OSC device is usually low ($EQE_{PV}<50\%$) or even no photocurrent is generated.[8,10] Although there are many factors influencing the free-carrier generation at D-A interfaces,[17] the manipulation of the hybridization between LE and CT states is one of the keys for simultaneously achieving high $EQE_{PV}$ and low $\Delta V_{nr}$.[18] Therefore, it is important to understand the correlation between LE-CT state intermixing and charge generation.

In this work, we focus on the impact of LE-CT hybridization on charge generation and recombination, employing steady-state photoluminescence (PL) and femtosecond transient absorption (fs-TA) spectroscopies. We manipulate the extent of hybridization by altering the $\Delta E_{LE-CT}$ values between the LE and CT states. We constructed two groups of material systems based on the electron donors PM6[19] and PTO2,[20] and electron acceptors C8IC[21] and Y6,[22] that is, PTO2:C8IC, PTO2:Y6, PM6:C8IC, and PM6:Y6 (**Figure 1**a). In contrast to the high-efficiency PM6:NFA blends, the PTO2:NFA blends exhibited smaller $EQE_{PV}$ (40–60%) in OSC devices; this was attributed to their smaller $\Delta E_{LE-CT}$ that results from the PTO2 ionization potential (IP) being 150 meV larger than that of PM6 (see Table S1, Supporting Information). In PTO2 blends, we found that the strong LE-CT hybridization can be identified from TA measurements. Ultra-fast CT state formation occurs via direct photoexcitation due to the increased oscillator strength of $S_0 \rightarrow CT$ transition. The CT states in such strong intermixed LE-CT states exhibit more local excitonic character, resulting in higher device electroluminescence and thus lower calculated $\Delta V_{nr}$, but also leading to barrierless back electron transfer and accelerated recombination pathways. In contrast, the PM6 blends with relatively weak LE-CT hybridization, show suppressed direct CT state formation, less radiative recombination, longer-lived CT and CS states, less impact of applied electric fields, and overall efficient charge generation. A key message from our work is that excessive LE-CT hybridization due to very small $\Delta E_{LE-CT}$ can suppress the ability of CT states to function as intermediates for highly efficient exciton-to-charge conversion.

## 2. Results and Discussion

### 2.1. Materials, Molecular Energetics, and Photovoltaic Performance

The chemical structures as well as absorption spectra of PM6, PTO2, C8IC, and Y6 are shown in Figure 1a and Figure S1, Supporting Information, respectively. C8IC has an acceptor-donor-acceptor (A-D-A) architecture. It differs from Y6, which exhibits an A-DAD-A architecture. Their state energies are estimated from cyclic voltammetry measurements and are listed in Table S1, Supporting Information.

In general, the extents of LE-CT hybridization and thermal population inversely depend on $\Delta E_{LE-CT}$,[9] which we adjusted by tuning the molecular energetics. As estimated from the IP offsets ($\Delta IP_{D-A}$) between donor and acceptor,[23] all four systems give $\Delta IP_{D-A} < 0.3$ eV and consequently small $\Delta E_{LE-CT}$ values. Since PTO2 exhibits a larger IP than PM6, the PTO2-based blends possess smaller $\Delta E_{LE-CT}$ values than those based on PM6. Moreover, it was confirmed that the enhancement of the electroluminescence quantum efficiencies ($EQE_{EL}$) of the devices was inversely correlated with $\Delta E_{LE-CT}$.[24] As shown in Figure 1b, the $EQE_{EL}$ values of PTO2-based devices ($2.3 \times 10^{-4}$ for PTO2:C8IC, $8.0 \times 10^{-4}$ for PTO2:Y6) are one order of magnitude higher than those of the PM6-based devices ($1.2 \times 10^{-5}$ for PM6:C8IC, $4.3 \times 10^{-5}$ for PM6:Y6); these $EQE_{EL}$ values are used to calculate the non-radiative voltage losses ($\Delta V_{nr}$) of the devices via the equation: $\Delta V_{nr} = -\frac{KT}{q}\ln(EQE_{EL})$,[25] as we discuss further below.

The photovoltaic performance of the devices is displayed in Figure 1c,d and Table S2, Supporting Information. Both PM6 blend devices displayed high efficiencies, with $EQE_{PV}$ above 70% extending to the near infrared. In contrast, the $EQE_{PV}$ and photocurrents of the PTO2 blend devices are relatively low. In order to make comparisons in photocurrent and voltage losses easier, we plotted the charge generation efficiencies (defined as $J_{SC}/J_{SC,SQ}$) as a function of $\Delta V_{nr}$,[26] since $\Delta V_{nr}$ has been one of the primary loss terms in OCSs, see Figure 1e. The corresponding data for the highest performing perovskite solar cells, giving a small $\Delta V_{nr}$ value (≈0.06 V) and a high quantum yield ($EQE_{PV}$> 90%),[27] are shown as a benchmark. In comparison to the PBDB-T:ITIC[28] and PTB7-Th:$PC_{71}BM$[6] systems that display large $\Delta E_{LE-CT}$ and large $\Delta V_{nr}$, PM6:C8IC and PM6:Y6 based systems show significant improvements by having lower $\Delta V_{nr}$ as well as higher $J_{SC}$ and $V_{OC}$. However, whilst both PTO2:C8IC and PTO2:Y6 devices exhibit even smaller $\Delta V_{nr}$ values and higher open-circuit voltages than the related PM6-based blends, their photocurrent densities and device fill factors are reduced. It should be noted that the PTO2:Y6 device shows much better photovoltaic performance than the PTO2:C8IC device, even though the former has the smaller $\Delta V_{nr}$. This point will be further discussed below.

### 2.2. Hybridization and Thermal Population Effects of the LE and CT States

For a deeper understanding of the impact that the LE-CT hybridization on the electronic states, we investigated the excited states of model PTO2:Y6, PM6:Y6, and PTO2:C8IC complexes (see Figure S2, Supporting Information) within the framework of time-dependent density functional theory (TD-DFT). Even though our modeling neglects aggregation effects, it provides a useful reference to gain insight into the interfacial electronic structure. The hole and electron natural transition orbitals (NTOs) in the three complexes are shown in **Figure 2**a–c while the energies and oscillator strengths (*f*) of the lowest excited states are given in Table S3, Supporting Information. The NTOwq2 analysis indicates that the first singlet excited state S1

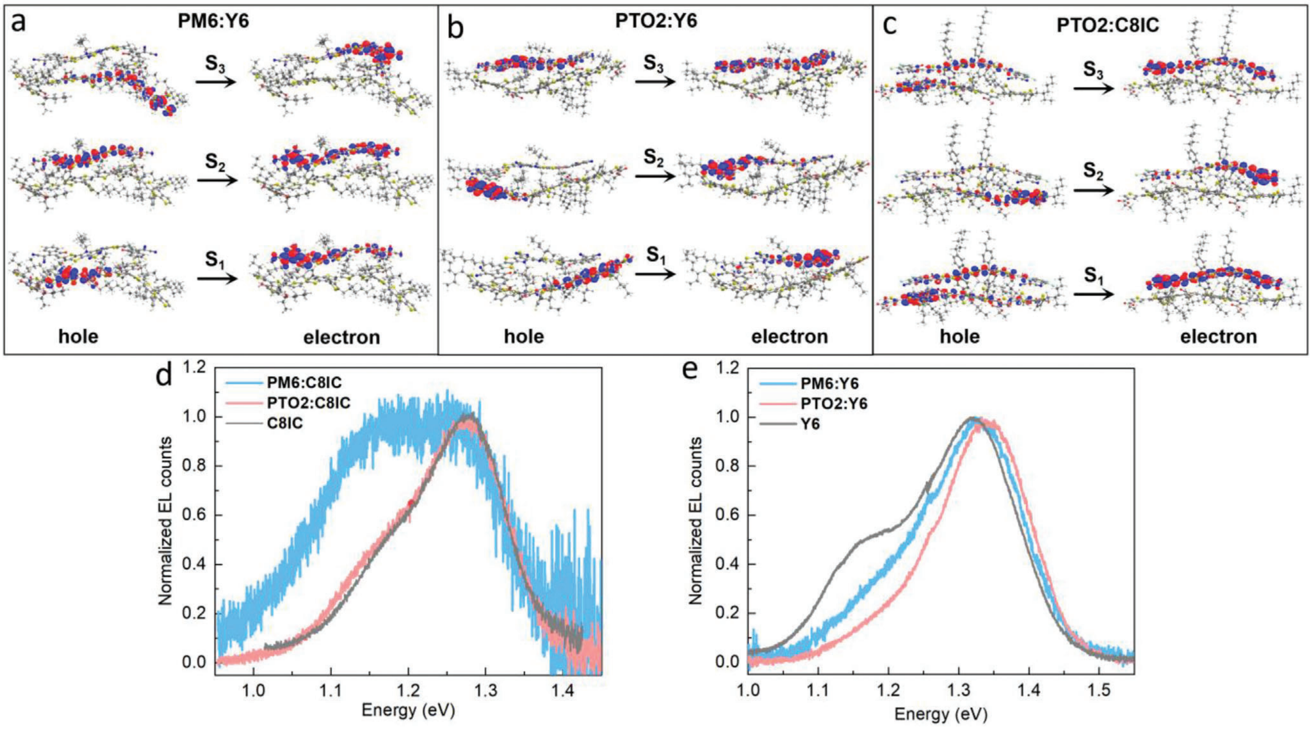

**Figure 2.** Hole and electron natural transition orbitals (NTOs) in the lowest three singlet excited states of the a) PM6:Y6, b) PTO2:Y6, and c) PTO2:C8IC complexes. d,e) Electroluminescent spectra of the devices based on D-A blend films (PM6:C8IC, PTO2:C8IC, PM6:Y6, and PTO2:Y6) and single-component films (C8IC and Y6).

in all blends has a CT character. We note that pure CT states are dark states, that is, they are characterized by a vanishing oscillator strength $f = 0$. $f$ values of 0.08 and 0.02 are estimated for the $S_1$ states in PTO2:Y6 and PM6:Y6, respectively, indicating a stronger hybridization of the CT state with the LE state in PTO2:Y6 than in PM6:Y6. The calculations also point to an even stronger LE-CT intermixing in PTO2:C8IC, in which the lower three excited states have very large $f$ values of 0.8, 0.4, and 1.0, respectively. These values and the NTOs shown in Figure 2c indicate that the CT and LE states are highly intermixed in this blend, that is, we cannot easily distinguish here between CT and LE state characters. This can be attributed primarily to the smaller $\Delta E_{\mathrm{LE-CT}}$ for the PTO2 blends. The resultant intermixed LE-CT states are radiatively coupled to the ground state, enabling direct optical excitation of these states via light absorption.

In our previous work, we found that the LE-CT hybridization and thermal population, described by a three-state model, jointly affect the emission properties of the blend films.[9] Electroluminescence (EL) studies were therefore conducted to further investigate the emission behaviors of the LE-CT states in the blends. In Figure 2d, the EL spectrum of PTO2:C8IC is observed to overlap well with that of neat C8IC. In contrast, in the PM6:C8IC blend, there is a strong emission peak emerging at 1.15 eV in addition to the main peak at 1.3 eV. In this PM6:C8IC blend, the low-energy peak is ascribed to CT emission and the high-energy peak, to optical transitions from thermally populated LE states. It is apparent that the CT energy in the PM6:C8IC blend is lower than that of the PTO2:C8IC blend, which is attributed to the larger IP of PTO2. As indicated by our DFT calculations, the extent of LE-CT intermixing is inversely dependent on $\Delta E_{\mathrm{LE-CT}}$. It is therefore expected to be stronger in PTO2:C8IC than PM6:C8IC, which is confirmed by the much higher $\mathrm{EQE_{EL}}$ of the PTO2:C8IC device. In Figure 2e, the EL spectra of PTO2:Y6 and PM6:Y6 do not show any additional emission in the low-energy region compared to the neat Y6. It turns out to be difficult to determine the CT-state energies from optical data in cases where the CT signals completely overlap those of singlet excitons due to a negligible $\Delta E_{\mathrm{LE-CT}}$. As discussed above, the $\mathrm{EQE_{EL}}$ of the PTO2:Y6 device ($8.0 \times 10^{-4}$) is much higher than that of PM6:Y6 ($4.3 \times 10^{-5}$); combined with estimations of their energy offsets from molecular state energies (Table S1, Supporting Information), we can infer that, compared to PM6:Y6, PTO2:Y6 exhibits enhanced radiative recombination due to the stronger LE-CT hybridization and thermal population effects. We note that although the LE-CT hybridization in PTO2:C8IC is stronger than in PTO2:Y6, the $\mathrm{EQE_{EL}}$ value of the PTO2:C8IC device is lower than that of the PTO2:Y6 device. The weaker LE-CT state intermixing but higher emission efficiency in the PTO2:Y6 device should be mainly attributed to the much higher photoluminescence quantum yield (PLQY) of Y6 (see Figure S3, Supporting Information). This emphasizes once again the importance of increasing the intrinsic PLQYs of the organic materials composing the active layer.[12]

### 2.3. Impact of LE-CT State Hybridization on CT Generation

In order to investigate further the variation in photocurrent generation efficiencies in the studied blends, we employed steady-state photoluminescence (PL) and femtosecond transient absorption (fs-TA) spectroscopies. PL quenching in blend films was characterized with respect to the PL of the corresponding polystyrene:NFA blend films. We evaluated the PL quenching of C8IC and Y6 by selectively exciting the NFAs at 780 nm, in which case exciton dissociation solely proceeds via hole transfer. Polystyrene (PS) is employed for diluting the NFA molecules, so as to mimic the morphology in a D-A blend and reduce the self-quenching induced by aggregation.[6] As displayed in **Figure 3**a,b, a significant amount of residual PL (≈40%) remains in the PTO2:NFA blends. In contrast, the PL of PM6:NFA blends is significantly quenched and only 9.5% (PM6:C8IC) and 2% (PM6:Y6) of residual PL remains. The PL intensities of PM6:NFA blend films are one order of magnitude lower than their PTO2:NFA counterparts, indicating that the excitons in PM6:NFA films have almost all converted to non-emissive CT and CS states. 2D grazing-incidence wide-angle X-ray scattering (GIWAXS) analyses show that the morphology of PM6:C8IC [PM6:Y6] and PTO2:C8IC [PTO2:Y6] are similar (see Figure S4, Supporting Information), which means that the higher residual PL of PTO2:NFA blends does not result from exciton decay in the bulk due to a rougher morphology. Rather, the higher PL of PTO2:NFA blends can be assigned to less efficient charge transfer and/or higher radiative efficiencies of LE-CT states in these blends.

As mentioned above, it is difficult to distinguish the CT emission from that of local excitons when these two electronic states are of nearly the same energy. We, therefore, carried out fs-TA measurements on the studied systems since TA is capable to trace exciton and CT signals separately.[29] Figure 3c–f shows the TA spectra of the PTO2:NFA blends and PM6:NFA blends at various pump-probe delay times. C8IC and Y6 are solely excited at a pump wavelength of 760 nm. The ground state bleaching (GSB) in the range of 650–780 nm was probed in all blends and can be ascribed to the GSB of the main optical transitions (i.e., ground state to exciton absorption) in C8IC and Y6 (Figure S5, Supporting Information). In addition, the bleaching signals peaking at 530 nm [580 nm] are similar to those observed for neat PTO2 [PM6] pumping at 525 nm (Figure S6, Supporting Information) and they can therefore be assigned to donor GSB signals. Considering that neat C8IC and Y6 films both display negligible signals below 650 nm and donor polymers are unable to absorb photons at 780 nm, we assign these donor GSB signals to CT states due to the hole transfer from NFA acceptor to polymer donor. In the case of the PM6:NFA blends, Figure 3c,d, the magnitude of the PM6 GSB (indicative of CT state formation) increases concomitantly with the decrease of the exciton signal (NFA bleaching) and reaches a maximum after 100 ps. This implies that the photogenerated excitons have efficiently transferred to CT states, which is consistent with the PL quenching results. In contrast, for PTO2:NFA blends, Figure 3e,f, the magnitude of the CT band (PTO2 GSB) is almost invariant (PTO2:Y6) or exhibits only a small increase (PTO2:C8IC) with time delay. Moreover, the CT signals in the PTO2 blends are much lower than their local-exciton signals, indicating inefficient exciton dissociation to CT states. The low CT generation in PTO2:NFA blends can be attributed to too strong a hybridization between the LE and CT states and the resultant dynamic equilibrium between the LE states and intermixed LE-CT states. Moreover, among the

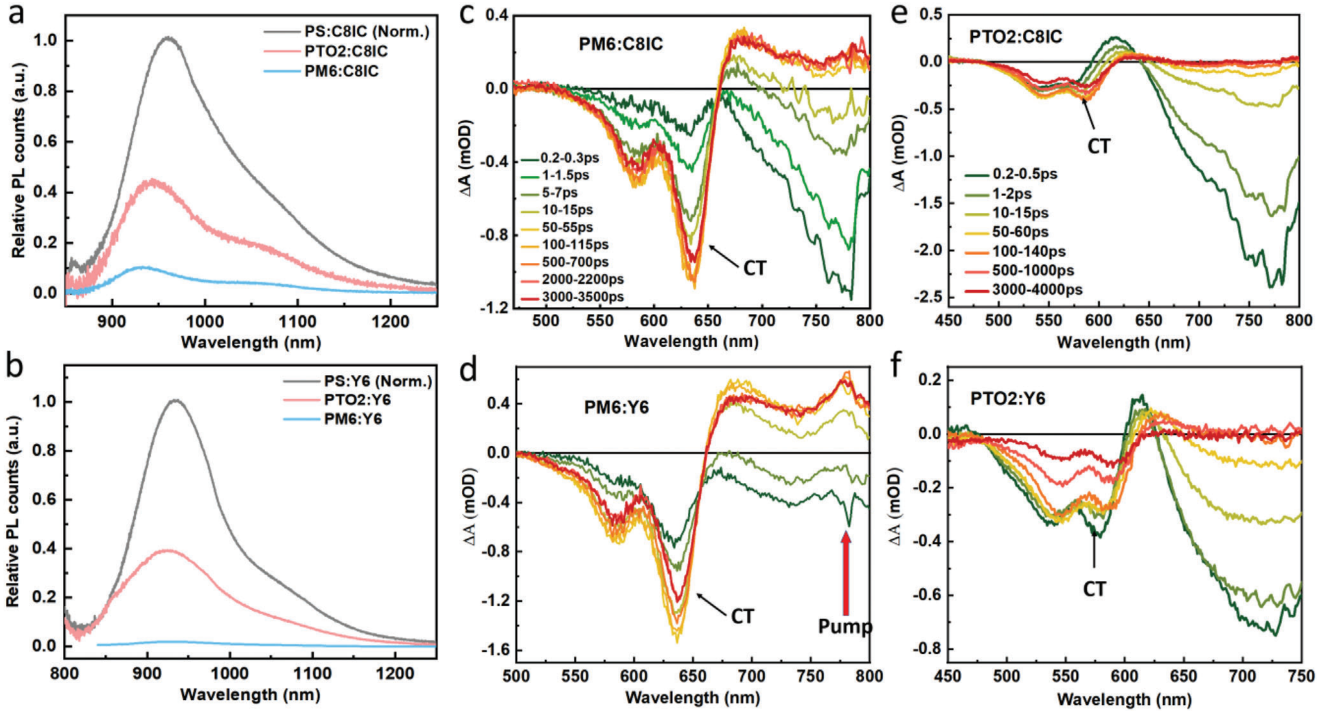

**Figure 3.** a,b) Steady-state PL quenching of the blends with respect to the neat films. The excitation is a continuous light $\lambda_{exc}$= 780 nm with intensity ≤100 mW cm$^{-2}$. The PL intensities of the films are calibrated by their absorptions at 780 nm. Transient absorption (TA) spectra in the visible region conducted on c) PM6:C8IC, d) PM6:Y6, e) PTO2:C8IC, and f) PTO2:Y6 with a pump at 760 nm (≤4 µJ cm$^{-2}$). The 2D TA spectra are shown in Figure S7, Supporting Information.

PTO2:NFA blends, the PTO2:C8IC blend appears to provide less CT generation than the PTO2:Y6 blend, owing to its stronger LE-CT hybridization.

### 2.4. Impact of LE-CT State Hybridization on the Kinetics of CT Generation and Charge Recombination

In this section, we focus on the kinetics of CT and CS states in PTO2:Y6 and PM6:Y6, see **Figure 4**a,b. The TA kinetics data for PTO2:C8IC and PM6:C8IC are shown in Figure S8a, Supporting Information, and have characteristics similar to those of the former two blends. It is apparent that the generation and decay kinetics of the CT and CS states in PTO2:Y6 are in stark contrast to those in PM6:Y6. In the PM6 blend, the growth of the PM6 GSB signals exhibits primarily a slow ($\tau_{grow}$ ≈ 10 ps) phase, assigned to the dynamics of exciton diffusion and charge transfer.[30] However, the PTO2 GSB signals in PTO2:Y6 are dominated by a prompt (primarily instrument response limited) growth within 400 fs. Following this instantaneous growth of the GSB is a fast decay. Pump fluence-dependent measurements (Figure 4b) show that these readily generated species are initially fluence independent up to 3 ps, indicative of a contribution from CT state (monomolecular) recombination.

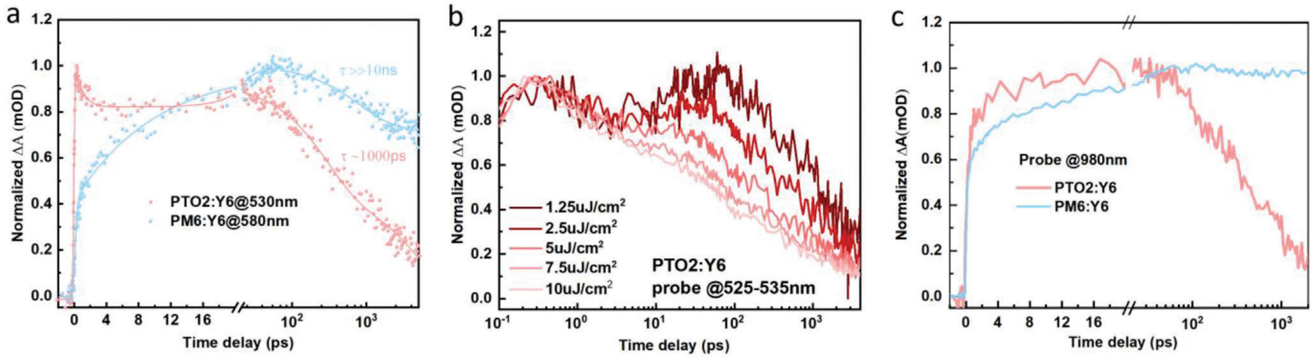

**Figure 4.** a) TA kinetics of PTO2:Y6 and PM6:Y6 blends upon pumping at 760 nm (≤4 µJ cm$^{-2}$) and probing at 530 nm (in purple) and 580 nm (in cyan). The solid lines are the global fitting curves. A biexponential function was utilized for fitting the decay stage and the extracted parameter $\tau$ represents the decay time of CT/CS species. b) Pump fluence-dependent TA kinetics probed at 525–535 nm for the PTO2:Y6 blend. c) TA kinetics of PTO2:Y6 and PM6:Y6 blends upon probing at 980 nm.

On longer time scales (>100 ps), the donor GSB signals decay, which is assigned to CT and CS states recombination (Figure 4a). It is apparent that the PM6:Y6 blend exhibits much slower (>10 ns) recombination kinetics than the PTO2:Y6 blend that shows an ≈1 ns decay pointing to accelerated recombination losses in this blend. This is consistent with our previous work demonstrating that the CT state lifetimes are shortened in systems with intermixed LE-CT states.[31] Furthermore, this difference in the timescale of recombination kinetics can also be observed when probing the excited-state absorption signal at 980 nm (Figure 4c). These ns decay kinetics were observed to be excitation density-dependent for both PM6:Y6[29] and PTO2:Y6 (Figure S9, Supporting Information and Figure 4b), indicative of bimolecular recombination of free carriers.

Our observation of the prompt CT-state generation in PTO2:Y6 is indicative of direct photoexcitation from the ground state to intermixed LE-CT states. This is consistent with the strong hybridization of LE and CT states in this blend seen in our DFT calculations. Analogous prompt CT formation was also observed in our TAS studies of PTO2:C8IC and in another small $\Delta E_{\mathrm{LE-CT}}$ blend PBDB-TCl:ITIC,[9] see Figure S8, Supporting Information. Our observation of faster charge recombination in PTO2:Y6 compared to PM6:Y6 is also consistent with greater hybridization of LE and CT states in the former. In this presence of strong hybridization, CT states are more coupled to localized, shorter-lived exciton states, rather than to delocalized CS states, in agreement with our observation of faster charge recombination for PTO2:Y6, PTO2:C8IC, and PBDB-TCl:ITIC (Figure S8, Supporting Information). As such, it can be concluded that whilst strong LE-CT mixing can enable direct, ultrafast CT state generation, it also provides pathways for accelerating charge recombination, lowering device performance.

It is striking that the very small $\Delta E_{\mathrm{LE-CT}}$ systems such as PTO2:Y6, whilst exhibiting accelerated recombination and lower device performance, also exhibit higher electroluminence yields and thus lower calculated $\Delta V_{\mathrm{nr}}$ (Figure 1). This can be understood by considering how $\mathrm{EQE_{EL}}$ depends on the radiative ($k_{\mathrm{r}}$) and non-radiative ($k_{\mathrm{nr}}$) recombination rate constants. Most simply, this dependence is given by $\mathrm{EQE_{EL}} = k_{\mathrm{r}}/(k_{\mathrm{r}} + k_{\mathrm{nr}})$.[32,33] On the one hand, solely suppressing the non-radiative rate constant results in an increased $\mathrm{EQE_{EL}}$, lower $\Delta V_{\mathrm{nr}}$, and high device performance, as has been reported in several studies.[34–36] However, an increased $\mathrm{EQE_{EL}}$ and lower $\Delta V_{\mathrm{nr}}$ can also result from increasing $k_{\mathrm{r}}$. In the case of all OSCs studied to date, $k_{\mathrm{r}}$ is much smaller than $k_{\mathrm{nr}}$ (as evidenced by $\mathrm{EQE_{EL}}$ values $<<1$).[9] The increase in $k_{\mathrm{r}}$ by itself will have only a marginal (detrimental) impact on device performance. We note that, as the CT states mediating recombination in OSCs do not normally contribute significantly to the overall absorption of solar irradiation, increasing $k_{\mathrm{r}}$ is not associated with an increase in light absorption,[37] in contrast to the situation in photovoltaic devices dominated by band-to-band light absorption and charge recombination. For the devices studied herein, the faster recombination kinetics in the presence of stronger LE-CT state hybridization can be understood as resulting from the shorter lifetime of LE states compared to CT states in most such blends (due to the increased overall, primarily non-radiative, recombination rate of local-excitons compared to CT states)[8,31,38] This further emphasizes the importance of the LE decay dynamics in small $\Delta E_{\mathrm{LE-CT}}$ OSCs, which is consistent with the recent study by Classen et al.[10]

### 2.5. Field-Dependent Charge Generation of LE-CT States

In order to investigate further the impact of LE-CT hybridization, steady-state PL spectra were collected for devices as a function of applied electrical bias. PL data for PTO:Y6, PM6:Y6, and neat Y6 devices in going from open-circuit (OC) to short-circuit (SC) conditions are shown in **Figure 5**a,b. It appears that 25% of the photoluminescence is quenched for the PTO2:Y6 device. Analogous behavior was observed for the PTO2:C8IC device (Figure S10a, Supporting Information). This contrasts to a single-component Y6 device, where the Y6 photoluminescence remains invariant (insert in Figure 5a).[39] Similar to neat Y6, PM6:Y6 (Figure 5b) and PM6:C8IC (Figure S10b, Supporting Information) devices also show invariant PL intensity from OC to SC conditions. The latter observation is typical of most OSCs,[40] and indicative of efficient, and field-independent, exciton separation into free charges in the blends with weak LE-CT hybridization. The field-dependent PL observed in PTO2 blends can be assigned to the impact of the built-in field on the intermixed LE-CT states in these blends, and means that a higher field can aid the separation of these strongly intermixed states into free charges.

As displayed in Figure 5c, the PL of a PTO2:Y6 device is increasingly quenched with higher reverse bias voltages. This quenching is much more pronounced than in the single-component device (insert in Figure 5c). Similar PL quenching trends with applied bias were also observed in the PTO2:C8IC device (Figure S11a, Supporting Information). To correlate the field driving PL quenching with photocurrent generation, field-dependent $\mathrm{EQE_{PV}}$ spectra were conducted as well, see Figure 5d and Figure S11b, Supporting Information. A $\mathrm{EQE_{PV}}$ enhancement with applied voltage appears in parallel with increased PL quenching. It should be noted that both field-dependent spectroscopic studies were observed to be reversible. It can be concluded that the yield of separated charges in these PTO2:NFA systems exhibits a high sensitivity toward external field, which is consistent with our previous work,[41] and can be assigned to the field dependence of separation of intermixed LE-CT states in these blends. This contrasts with relatively larger energy offset and less intermixed LE-CT states in the PM6:NFA systems, which do not exhibit a strong field dependence of their photophysics (Figure S12, Supporting Information). We also note that the field dependence of the PL quenching in PTO2:C8IC is less pronounced than in PTO2:Y6, which is again due to the stronger coupling between the LE and CT states in PTO2:C8IC. In addition, the enhanced field dependence for the PTO2 blend devices is also consistent with their lower device fill factors (FF), which are determined by the competition between charge extraction and recombination.[42] As shown in Figure 5e, the PTO2:Y6, PTO2:C8IC, and PBDB-TCl:ITIC devices all present lower FF than their PM6:Y6, PM6:C8IC, and PBDB-T:ITIC[9] counterparts, which correlates with lower $\Delta V_{\mathrm{nr}}$ values, as a result of strengthened LE-CT hybridization.

In order to reveal the mechanism behind an electric-field driven LE-CT state dissociation, we computed the excited states of a PTO2:Y6 complex in the presence of an applied external

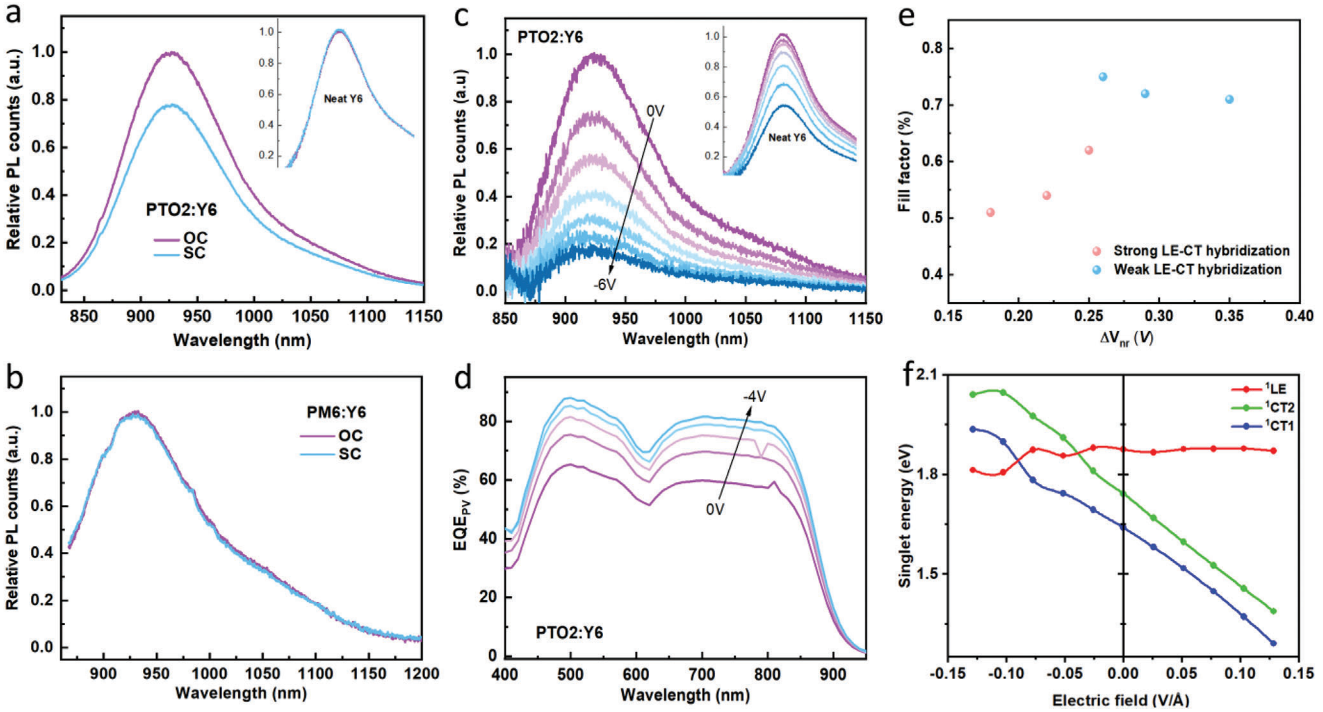

**Figure 5.** Electric field-dependent PL measurements from OC to SC for a) PTO2:Y6 and neat Y6 (insert) devices and b) PM6:Y6 device. Electric field-dependent measurements of the device based on PTO2:Y6 for c) PL and d) EQE$_{PV}$ upon reverse bias voltages. The excitation is a continuous light $\lambda_{exc}$= 780 nm with intensity $\leq$ 100 mW cm$^{-2}$ (1 sun). The active-layer thicknesses in all devices are around 100 nm, guaranteeing similar electric field densities across the BHJ films under the same applied voltages. e) Fill factor versus $\Delta V_{nr}$ of devices based on PTO2:Y6, PTO2:C8IC, PBDB-TCl:ITIC,[9] PM6:Y6, PM6:C8IC, and PBDB-T:ITIC.[9] f) Impact of an electric field on the calculated energies of singlet LE-CT states; the external electric field ($F_Z$) was applied along the PTO2 to Y6 (+Z) direction or along the reverse direction.

electric field ($F_Z$) along the direction perpendicular to the molecular planes (see Figure S13, Supporting Information). The results show that an increasing positive electric field (see Figure 5f) widens the LE-CT (as well as LE-CS) energy gap while it has only a minor effect on the LE state energy. As a result, exciton dissociation is expected to be enhanced by the electric field. We note that, since the orientations of the D and A (macro)molecules are somewhat random, the LE-CT gaps of some PTO2:Y6 pairs can decrease or even become negative. However, due to energy migration, excitons on these pairs will funnel into the D:A pairs with increased LE-CT gaps and dissociate. The same mechanism is expected to be operative in single-component devices, that is, the intermolecular CT states as well as the CS states stabilized by the electric field can promote exciton dissociation, as is confirmed by PL quenching.

## 3. Discussion

In summary, we have demonstrated that a very small $\Delta E_{LE-CT}$ results in stronger LE-CT state hybridization, higher EQE$_{EL}$, faster but lower CT state generation, and faster charge recombination. We found that such strong LE-CT intermixing can be weakened by the application of an electric field, which enhances the yield of CT and CS states, but attenuates the emission efficiency of the device. We can therefore conclude that too strong a hybridization of the LE and CT states reduces the non-radiative voltage loss of the device mainly as a result of an increased radiative recombination rather than a suppression of non-radiative recombination. Thus, it negatively impacts the ability of CT states to function as efficient intermediates for exciton-to-charge conversion. From the comparison between the PTO2:Y6 and PTO2:C8IC blends, we also learn that the trade-off between EQE$_{PV}$ and EQE$_{EL}$ in an OSC is not only affected by the LE-CT state hybridization, but also by the intrinsic properties of the organic materials, such as their PLQY and PL lifetime.[10] Interestingly, a recent study demonstrated a useful way to further reduce the trade-off by introducing asymmetric acceptors, in which one end of the acceptor leads to a CT state with a larger offset, which is beneficial for charge generation, while the other end of the acceptor leads to a CT state with a very small offset, which is beneficial for electroluminescence.[43]

## 4. Experimental Section

*Materials*: The studied materials were all commercially purchased from the company of Solarmer Materials, Inc.

*Fabrication of Films and Devices*: The device configuration was as follows: Indium tin oxide/ZnO/active layer/MoO3/Ag. The D-A (or PS-NFA) blend solutions of the studied systems were prepared with D/A weight ratio of 1:1.2 and total concentration of 18 mg mL$^{-1}$, dissolved in chloroform with 0.5% additive of diphenyl sulfide for C8IC blends or chloronaphthalene for Y6 blends. The films were thermally annealed at 100 °C for 5 min (C8IC blends) or 10 min (Y6 blends) following the spin-coating process. The films for PL and TA measurements were fabricated from the same solutions, as that for the devices, with spin-coating on glass followed by thermal annealing and studied in $N_2$ atmospheres.

*J–V and $EQE_{PV}$ Characterizations*: More than 10 devices (40 pixels) were characterized for each material system. The *J–V* curves were collected by using a Keithley 2400 Source Meter under AM1.5 illumination provided by a solar simulator (LSH-7320 ABA LED solar simulator) with an intensity of 1,000 W $m^{-2}$ after spectral mismatch correction. The light intensity for the *J–V* measurements was calibrated with a reference silicon cell (VLSI standards SN 10510-0524 certified by National Renewable Energy Laboratory). The EQE spectra were recorded by an integrated quantum efficiency measurement system named QE-R3011 (Enli Technology), which was calibrated with a crystalline silicon photovoltaic cell before use. Field-dependent $EQE_{PV}$ spectra were measured using an integrated system from Quantum Design PV300. All devices were sealed and tested in ambient air.

*$EQE_{EL}$ Measurement*: $EQE_{EL}$ was measured by a home-built system with a Hamamatsu silicon photodiode 1010B. A Keithley 2400 was employed as bias voltage supplier and recording injected current. A Keithley 485 was used for collecting the photocurrent generated from the emitted photons of the samples.

*PL Measurement*: PL/EL spectra were recorded by an Andor spectrometer (a Shamrock sr-303i-B Spectrograph). Andor iDus camera of iDus InGaAs array in the infrared range from 900 to 1,600 nm was employed by cooling down to −90 °C. An Oriel liquid light guide from Newport (Irvine) was then connected to the entrance slit of the spectrometer and the other end was placed as close as possible to the active area of the samples. The system was wavelength calibrated by an argon lamp to a resolution better than 0.5 nm. The lineshapes of the recorded spectra were calibrated by an Optronic OL245 м standard spectral irradiance lamp. Field-dependent PL was conducted on devices connecting to an external current/voltage source meter Keithley 2400. A laser diode with wavelength of 780 nm was used as excitation light source.

*Femtosecond TA Measurement*: A broadband pump-probe femtosecond (fs) transient absorption (TA) spectrometer Helios (Spectra Physics, Newport Corp.) was used to measure the TA spectra and kinetics for the studied sample films. Ultrafast laser pulses (800 nm, 100 fs duration) were generated by a 1 kHz Ti:sapphire regenerative amplifier (Solstice, Spectra Physics, Newport Corp.). One portion of the 800 nm pulse was guided to an optical parametric amplifier (TOPAS Prime, Spectra-Physics) and a frequency mixer (Niruvis, Light Conversion) to tune the pump pulses of 750–800 nm for the measurements. The pump pulses were modulated at a frequency of 500 Hz by a mechanical chopper. The rest of the 800 nm pulse was routed onto a mechanical delay stage with a 6 ns time window and directed through a non-linear crystal (sapphire for the visible region) to generate a white light probe ranging from 400–800 nm. The probe pulse was split into two by a neutral density filter. One probe pulse acted as the reference and was directly sent to the fiber-optic coupled multichannel spectrometers (CCD Si detector). Another probe pulse together with the pump pulse was focused onto the same spot on the sample films with a beam area of around 0.5 $mm^2$ before sending it to the spectrometer. To compensate for fluctuations, the measured spectrum was normalized to the reference spectrum and averaged for several scans to achieve a good signal-to-noise ratio. Data analysis was performed with the commercialized Surface Xplorer software.

*Computational Details*: The geometry optimizations of the PTO2:Y6, PM6:Y6, and PTO2:C8IC complexes were carried out by means of DFT using the long-range corrected $\omega$B97XD functional in combination with a 6–31g(d) basis set. The PTO2 and PM6 polymer chains were represented by trimers and dimers, respectively. The side chains on the donor and acceptor molecules were known to be crucial for an accurate description of interchromophoric distances and interactions, which in turn control the overall electronic processes in the OSC; thus, they were taken into account during the geometry optimization process. It was noted that derived in this way geometries (Figure S2, Supporting Information) resemble very well the dominant D:A interface conformations, as previously proven for PM6:Y6 and other D:A blends by means of molecular dynamics simulations and experimental techniques.[44–46] The excited-state properties of the energy-minimized structures were evaluated using TD-DFT at the $\omega$B97XD/6-31G(d,p) level of theory. The range-separation parameter $\omega$ was taken as 0.01 $\text{Bohr}^{-1}$ according to the previous work.[43,47] An implicit dielectric environment based on the polarizable continuum model was considered during the TD-DFT calculations. The dielectric constant ($\epsilon$) was taken as 3.0, a typical value for active layers in an OSC. The impact of an electrical field on the excited-state properties was considered by applying an external field ($F_Z$) along the direction perpendicular to the molecular planes. The field strength was varied from 0.0 to ± 0.15 V $Å^{-1}$ with a step size of 0.03 V $Å^{-1}$. The nature of the excited states was visualized by analyzing the NTOs. All the calculations were performed using the Gaussian 16 package.[48]

## Supporting Information

Supporting Information is available from the Wiley Online Library or from the author.

## Acknowledgements

The authors thank Wolfgang Tress, Chunfeng Zhang for useful discussions, and Alexander J. Gillett for supplying TA data. D.Q. was supported by the Swedish Research Council VR (grant no. 2019-00677). M.Z. acknowledges financial support from the National Natural Science Foundation of China (NSFC) (no. 51973146), the Shandong Provincial Natural Science Foundation (ZR2022JQ09), and the Collaborative Innovation Center of Suzhou Nano Science & Technology. J.R.D. and N.G. thanks the EPSRC project ATIP (EP/TO28513/1) for financial support. The work at Arizona was supported by the Office of Naval Research, award no. N00014-20-1-2110.

## Conflict of Interest

The authors declare no conflict of interest.

## Author Contributions

D.Q., F.G., and J.R.D. conceived and directed the project. D.Q. fabricated the solar cell devices, performed the *J–V*, $EQE_{PV}$, steady-state photoluminescence, electroluminescence, $EQE_{EL}$, and transient absorption experiments. S.M.P., V.C., and J.-L.B. carried out the DFT calculations. Q.L. and X.G. fabricated the solar cell devices, performed the *J–V*, $EQE_{PV}$. Y.D. performed the TA measurements. R.Z. measured the GIWAXS. N.G. and J.W. measured the field-dependent $EQE_{PV}$. T.Z. fabricated the devices. M.Z. provided the initial data for the start of the project and participated in the data analysis. D.Q., S.M.P., V.C., F.G., and J.R.D. wrote the manuscript. All authors contributed to the discussion and finalized the manuscript.

## Data Availability Statement

The data that support the findings of this study are available from the corresponding author upon reasonable request.

## Keywords

charge generation, hybridization, non-radiative voltage loss, organic solar cells

Received: April 5, 2023
Revised: June 22, 2023
Published online: July 21, 2023

[1] C. Li, J. Zhou, J. Song, J. Xu, H. Zhang, X. Zhang, J. Guo, L. Zhu, D. Wei, G. Han, *Nat. Energy* **2021**, *6*, 605.
[2] K. Chong, X. Xu, H. Meng, J. Xue, L. Yu, W. Ma, Q. Peng, *Adv. Mater.* **2022**, *34*, 2109516.
[3] L. Zhu, M. Zhang, J. Xu, C. Li, J. Yan, G. Zhou, W. Zhong, T. Hao, J. Song, X. Xue, *Nat. Mater.* **2022**, *21*, 656.
[4] K. Jiang, J. Zhang, C. Zhong, F. R. Lin, F. Qi, Q. Li, Z. Peng, W. Kaminsky, S.-H. Jang, J. Yu, *Nat. Energy* **2022**, 7, 1076.
[5] A. Karki, A. J. Gillett, R. H. Friend, T. Q. Nguyen, *Adv. Energy Mater.* **2020**, *11*, 2003441.
[6] D. Qian, Z. Zheng, H. Yao, W. Tress, T. R. Hopper, S. Chen, S. Li, J. Liu, S. Chen, J. Zhang, *Nat. Mater.* **2018**, *17*, 703.
[7] J. Liu, S. Chen, D. Qian, B. Gautam, G. Yang, J. Zhao, J. Bergqvist, F. Zhang, W. Ma, H. Ade, *Nat. Energy* **2016**, *1*, 16089.
[8] F. D. Eisner, M. Azzouzi, Z. Fei, X. Hou, T. D. Anthopoulos, T. J. S. Dennis, M. Heeney, J. Nelson, *J. Am. Chem. Soc.* **2019**, *141*, 6362.
[9] X.-K. Chen, D. Qian, Y. Wang, T. Kirchartz, W. Tress, H. Yao, J. Yuan, M. Hülsbeck, M. Zhang, Y. Zou, *Nat. Energy* **2021**, 6, 799.
[10] A. Classen, C. L. Chochos, L. Lüer, V. G. Gregoriou, J. Wortmann, A. Osvet, K. Forberich, I. McCulloch, T. Heumüller, C. J. Brabec, *Nat. Energy* **2020**, *5*, 711.
[11] R. Shivhare, G. J. Moore, A. Hofacker, S. Hutsch, Y. Zhong, M. Hambsch, T. Erdmann, A. Kiriy, S. C. Mannsfeld, F. J. A. m. Ortmann, *Adv. Mater.* **2022**, *34*, 2101784.
[12] V. Coropceanu, X.-K. Chen, T. Wang, Z. Zheng, J.-L. Brédas, *Nat. Rev. Mater.* **2019**, *4*, 689.
[13] K. Vandewal, *Annu. Rev. Phys. Chem.* **2016**, *67*, 113.
[14] T. M. Clarke, J. R. Durrant, *Chem. Rev.* **2010**, *110*, 6736.
[15] K. Vandewal, S. Mertens, J. Benduhn, Q. Liu, *J. Phys. Chem. Lett.* **2019**, *11*, 129.
[16] H. Lu, W. Liu, H. Jin, H. Huang, Z. Tang, Z. J. A. F. M. Bo, Adv. Funct. Mater. **2022**, *32*, 2107756.
[17] F. Gao, O. Inganäs, *Phys. Chem. Chem. Phys.* **2014**, *16*, 20291.
[18] J. Yuan, T. Huang, P. Cheng, Y. Zou, H. Zhang, J. L. Yang, S.-Y. Chang, Z. Zhang, W. Huang, R. Wang, *Nat. Commun.* **2019**, *10*, 570.
[19] M. Zhang, X. Guo, W. Ma, H. Ade, J. Hou, *Adv. Mater.* **2015**, *27*, 4655.
[20] H. Yao, Y. Cui, D. Qian, C. S. Ponseca Jr, A. Honarfar, Y. Xu, J. Xin, Z. Chen, L. Hong, B. Gao, *J. Am. Chem. Soc.* **2019**, *141*, 7743.
[21] Y. Chen, T. Liu, H. Hu, T. Ma, J. Y. L. Lai, J. Zhang, H. Ade, H. Yan, *Adv. Energy Mater.* **2018**, *8*, 1801203.
[22] J. Yuan, Y. Zhang, L. Zhou, G. Zhang, H.-L. Yip, T.-K. Lau, X. Lu, C. Zhu, H. Peng, P. A. Johnson, *Joule* **2019**, *3*, 1140.
[23] J. Zhang, W. Liu, G. Zhou, Y. Yi, S. Xu, F. Liu, H. Zhu, X. Zhu, *Adv. Energy Mater.* **2019**, *10*, 1903298.
[24] Y. Xie, W. Wang, W. Huang, F. Lin, T. Li, S. Liu, X. Zhan, Y. Liang, C. Gao, H. Wu, *Energy Environ. Sci.* **2019**, *12*, 3556.
[25] U. Rau, *Phys. Rev. B* **2007**, *76*, 085303.
[26] L. Krückemeier, U. Rau, M. Stolterfoht, T. Kirchartz, *Adv. Energy Mater.* **2020**, *10*, 1902573.
[27] J. Jeong, M. Kim, J. Seo, H. Lu, P. Ahlawat, A. Mishra, Y. Yang, M. A. Hope, F. T. Eickemeyer, M. Kim, *Nature* **2021**, *592*, 381.
[28] W. Zhao, D. Qian, S. Zhang, S. Li, O. Inganäs, F. Gao, J. Hou, *Adv. Mater.* **2016**, *28*, 4734.
[29] R. Wang, C. Zhang, Q. Li, Z. Zhang, X. Wang, M. Xiao, *J. Am. Chem. Soc.* **2020**, *142*, 12751.
[30] Y. Zhong, M. Causa, G. J. Moore, P. Krauspe, B. Xiao, F. Günther, J. Kublitski, R. Shivhare, J. Benduhn, E. BarOr, *Nat. Commun.* **2020**, *11*, 833.
[31] Y. Dong, H. Cha, H. L. Bristow, J. Lee, A. Kumar, P. S. Tuladhar, I. McCulloch, A. A. Bakulin, J. R. Durrant, *J. Am. Chem. Soc.* **2021**, *143*, 7599.
[32] J. Benduhn, K. Tvingstedt, F. Piersimoni, S. Ullbrich, Y. Fan, M. Tropiano, K. A. McGarry, O. Zeika, M. K. Riede, C. J. Douglas, *Nat. Energy* **2017**, *2*, 17053.
[33] M. Azzouzi, J. Yan, T. Kirchartz, K. Liu, J. Wang, H. Wu, J. Nelson, *Phys. Rev. X* **2018**, *8*, 031055.
[34] J. Wang, X. Jiang, H. Wu, G. Feng, H. Wu, J. Li, Y. Yi, X. Feng, Z. Ma, W. Li, *Nat. Commun.* **2021**, *12*, 6679.
[35] X. K. Chen, J. L. Brédas, *Adv. Energy Mater.* **2018**, *8*, 1702227.
[36] B. Blank, T. Kirchartz, S. Lany, U. Rau, *Phys. Rev. Appl.* **2017**, *8*, 024032.
[37] K. Vandewal, K. Tvingstedt, A. Gadisa, O. Inganäs, J. V. Manca, *Phys. Rev. B* **2010**, *81*, 125204.
[38] R. Shivhare, G. J. Moore, A. Hofacker, S. Hutsch, Y. Zhong, M. Hambsch, T. Erdmann, A. Kiriy, S. C. Mannsfeld, F. Ortmann, *Adv. Mater.* **2022**, *34*, 2101784.
[39] K. Tvingstedt, K. Vandewal, F. Zhang, O. Inganäs, *J. Phys. Chem. C* **2010**, *114*, 21824.
[40] K. Vandewal, Z. Ma, J. Bergqvist, Z. Tang, E. Wang, P. Henriksson, K. Tvingstedt, M. R. Andersson, F. Zhang, O. Inganäs, *Adv. Funct. Mater.* **2012**, *22*, 3480.
[41] V. C. Nikolis, Y. Dong, J. Kublitski, J. Benduhn, X. Zheng, C. Huang, A. C. Yüzer, M. Ince, D. Spoltore, J. R. Durrant, *Adv. Energy Mater.* **2020**, *10*, 2002124.
[42] D. Bartesaghi, I. D. C. Pérez, J. Kniepert, S. Roland, M. Turbiez, D. Neher, L. Koster, *Nat. Commun.* **2015**, *6*, 7083.
[43] C. He, Z. Chen, T. Wang, Z. Shen, Y. Li, J. Zhou, J. Yu, H. Fang, Y. Li, S. Li, *Nat. Commun.* **2022**, *13*, 2598.
[44] G. Zhang, X. K. Chen, J. Xiao, P. C. Y. Chow, M. Ren, G. Kupgan, X. Jiao, C. C. S. Chan, X. Du, R. Xia, Z. Chen, J. Yuan, Y. Zhang, S. Zhang, Y. Liu, Y. Zou, H. Yan, K. S. Wong, V. Coropceanu, N. Li, C. J. Brabec, J. L. Bredas, H. L. Yip, Y. Cao, *Nat. Commun.* **2020**, *11*, 3943.
[45] Y. Liu, Z. Zheng, V. Coropceanu, J. L. Bredas, D. S. Ginger, *Mater. Horiz.* **2022**, *9*, 325.
[46] B. R. Luginbuh, P. Raval, T. Pawlak, Z. Du, T. Wang, G. Kupgan, N. Schopp, S. Chae, S. Yoon, A. Yi, H. Jung Kim, V. Coropceanu, J. L. Bredas, T. Q. Nguyen, G. N. M. Reddy, *Adv. Mater.* **2022**, *34*, 2105943.
[47] T. Wang, V. Coropceanu, J.-L. Brédas, *Chem. Mater.* **2019**, *31*, 6239.
[48] M. Frisch, G. Trucks, H. Schlegel, G. Scuseria, M. Robb, J. Cheeseman, G. Scalmani, V. Barone, G. Petersson, H. Nakatsuji, X. Li, M. Caricato, A. V. Marenich, J. Bloino, B. G. Janesko, R. Gomperts, B. Mennucci, H. P. Hratchian, J. V. Ortiz, A. F. Izmaylov, J. L. Sonnenberg, D. Williams-Young, F. Ding, F. Lipparini, F. Egidi, J. Goings, B. Peng, A. Petrone, T. Henderson, D. Ranasinghe, et al., Gaussian, Inc., Wallingford, CT **2016**.